








Tuning the magnetocaloric effect in the Lu-doped frustrated Shastry-Sutherland system TmB_4

Mat. Orendáč ¹, P. Farkašovský,¹ L. Regeciová ¹, S. Gabáni ¹, G. Pristáš ¹, E. Gažo ¹, J. Bačkai ², P. Diko,¹
A. Dukhnenko,³ N. Shitsevalova,³ K. Siemensmeyer,⁴ and K. Flachbart ¹

¹*Institute of Experimental Physics, Slovak Academy of Sciences, Watsonova 47, 04001 Košice, Slovakia*

²*Faculty of Electrical Engineering and Informatics, Technical University, Letná 9, 04200 Košice, Slovakia*

³*Institute for Problems of Materials Science, National Academy of Sciences of Ukraine, Krzhynanovskyy 3, 03680 Kiev, Ukraine*

⁴*Helmholtz-Zentrum Berlin, Hahn-Meitner Platz 1, 14109 Berlin, Germany*



(Received 29 July 2020; revised 8 October 2020; accepted 23 October 2020; published 12 November 2020)

TmB_4 is an anisotropic, metallic magnetic system with geometrical frustration of the Shastry-Sutherland type. Here an experimental study of the magnetocaloric effect (MCE) in Lu-doped $\text{Tm}_{1-x}\text{Lu}_x\text{B}_4$ ($x = 0.06, 0.30$), evaluated from the temperature dependence of heat capacity and magnetization curves at 2 K, is presented. The results are described within a theoretical model based on an extended Ising Hamiltonian which considers interactions up to the fourth-next-nearest neighbors. Model parameters were optimized to achieve the best match to the experimental results over the whole range of Lu^{3+} ion concentrations. After optimization a good quantitative agreement with the adiabatic temperature change and a good qualitative agreement with magnetization curves is obtained. Our study shows that the efficiency of the MCE can be tuned by dilution with nonmagnetic Lu ions. The theoretical model developed could be used to design new magnetocaloric materials.

DOI: [10.1103/PhysRevB.102.174422](https://doi.org/10.1103/PhysRevB.102.174422)

I. INTRODUCTION

The magnetocaloric effect (MCE) represents a magnetothermodynamic phenomenon where the temperature variation of a magnetic material is caused by the change of the external magnetic field [1–6]. Due to high efficiency and environmentally friendly operation of MCE based refrigeration in comparison with compression-expansion principle it still attracts much attention.

Thulium tetraboride (TmB_4) is an anisotropic geometrically frustrated magnetic system, which belongs to the group of rare-earth tetraborides (REB_4) that crystallize in a tetragonal lattice [7–9]. These compounds are good metals and the RKKY exchange interaction between the magnetic ions plays an important role. In the case of TmB_4 the magnetic Tm^{3+} ions have a $4f^{12}$ configuration with an angular momentum $J = 6$ while in the case of LuB_4 nonmagnetic Lu^{3+} ions have a closed electron configuration $4f^{14}$. Therefore, by replacing magnetic Tm^{3+} ions with nonmagnetic Lu^{3+} ions the magnetic system is diluted and around the impurity magnetic bonds are broken. In the mentioned tetragonal lattice the RE ions lie in sheets perpendicular to the c axis and can be mapped within this (a – b) plane onto the frustrated Shastry-Sutherland lattice (SSL), which can be viewed in terms of squares and equilateral triangles [10–14]. These Tm (Lu) sheets are separated by planes of boron atoms grouped into B_6 octahedra and dimer pairs. Due to the crystal-field effect on Tm^{3+} sites, the degeneracy of the $J = 6$ multiplet is lifted leading to the ground state doublet $M_J = \pm 6$. This induces a strong Ising-like magnetic anisotropy where the magnetic moments of the Tm ions are oriented along the c axis below the Néel temperature of $T_N = 11.7$ K. The strong anisotropy

of this system is seen comparing the field magnitudes necessary for spin saturation. In the case of $H \parallel c$, a field of 40 kOe is needed to reach the saturation, while for case $H \perp c$ this field is above 300 kOe [10]. In the magnetization curve of TmB_4 also various plateaus were observed with values $1/2$, $1/8$ of the saturation magnetization M_{sat} [12,15]. Recently it was argued that the $1/8$ plateau is metastable, arising because the spin dynamics is frozen below $T \approx 4.5$ K [15,16].

The strong crystal-field effects allow a description of TmB_4 in terms of an effective spin $1/2$ Shastry-Sutherland model with a strong Ising anisotropy [12]. As a first approach for an explanation of magnetization processes in metallic Shastry-Sutherland magnets, the Ising model on the SSL was used. This model has been solved numerically [17,18] as well as analytically [19] with the conclusion that only the $M/M_{\text{sat}} = 1/3$ plateau is stabilized by J_1 and J_2 interactions which is not observed experimentally. This discrepancy led to the introduction of a third-nearest-neighbor interaction J_3 in the model [20]. The Ising model was extended with the addition of a J_4 interaction [21–23]. Effects of long-range interactions on ground-state structures in Ising magnets on the Shastry-Sutherland lattice were studied in detail in [24]. The observed fractional magnetization plateaus in TmB_4 were also explained by Kondo-Ising and tight-binding models [25]. These studies led to the conclusion that long-range interactions can play a crucial role in the stabilization of different magnetization plateaus with fractional magnetization values. The magnetocaloric properties of TmB_4 were studied in [26,27] and are described theoretically in [28]. Effects of doping on magnetocaloric properties of a different tetraboride $\text{Ho}_{1-x}\text{Dy}_x\text{B}_4$ ($x = 0.0, 0.5, \text{ and } 1.0$) have been reported recently in [29].

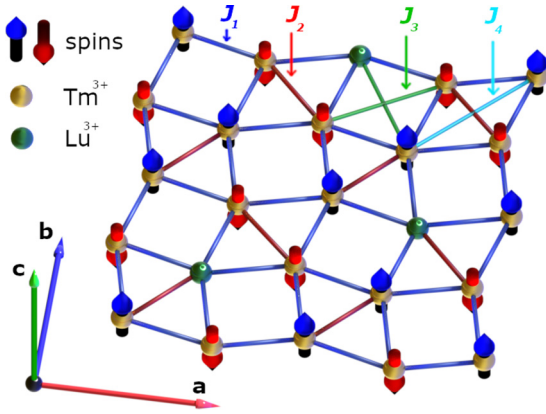


FIG. 1. Diluted Shastry-Sutherland lattice with interactions up to fourth-next-nearest neighbors.

The aim of this work is the investigation of magnetocaloric properties in TmB_4 as a result of its dilution by nonmagnetic Lu ions. We present an experimental study of the MCE in $\text{Tm}_{1-x}\text{Lu}_x\text{B}_4$ ($x = 0.06, 0.30$) solid solutions evaluated from measurements of the temperature-dependent heat capacity. Also the magnetization at 2 K is investigated. For the microscopic description of the experimental results a theoretical model based on the extended Ising Hamiltonian is used. It considers interactions up to the fourth-next-nearest neighbors (see Fig. 1) [30]. Due to the similar ionic radius of the Tm and Lu ions changes of the lattice geometry are not expected over the whole range of concentrations. Therefore, one set of exchange parameters J_1, J_2, J_3 , and J_4 was used for all cases. After optimization of the model parameters a good match with the experimental results is obtained. From the tuned model it is possible to predict an optimal concentration x for best magnetocaloric properties.

II. MATERIALS AND METHODS

$\text{Tm}_{1-x}\text{Lu}_x\text{B}_4$ ($x = 0.0, 0.06$, and 0.30) single crystals were grown by an inductive, crucible-free zone melting method. The high residual resistivity ratios (30, 9, and 7) point to their high quality. For heat-capacity and magnetization measurements the samples were oriented and cut to dimensions of approximately $1 \times 1 \times 0.5 \text{ mm}^3$. The temperature dependence of the heat capacity was measured between 2 and 40 K in various magnetic fields up to 48 kOe. A commercial Quantum Design PPMS system with the relaxation method was used. All measurements were performed for a field orientation $H \parallel c$, and for every experimental point the temperature and magnetic field was stabilized. The field dependence of the magnetization at 2 K in the field range 0–50 kOe was measured in a commercial Quantum Design MPMS system using the RSO option.

III. RESULTS AND DISCUSSION

A. Low-temperature thermodynamic properties of variously doped $\text{Tm}_{1-x}\text{Lu}_x\text{B}_4$ single crystals

The low-temperature thermodynamic properties of $\text{Tm}_{1-x}\text{Lu}_x\text{B}_4$ single crystals were evaluated from

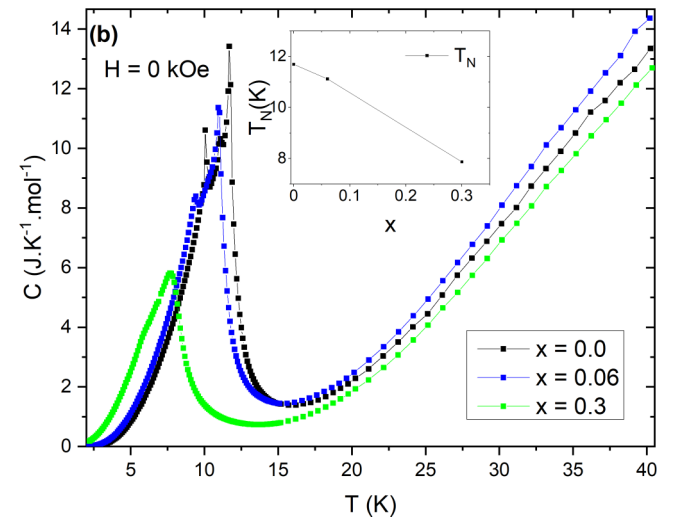
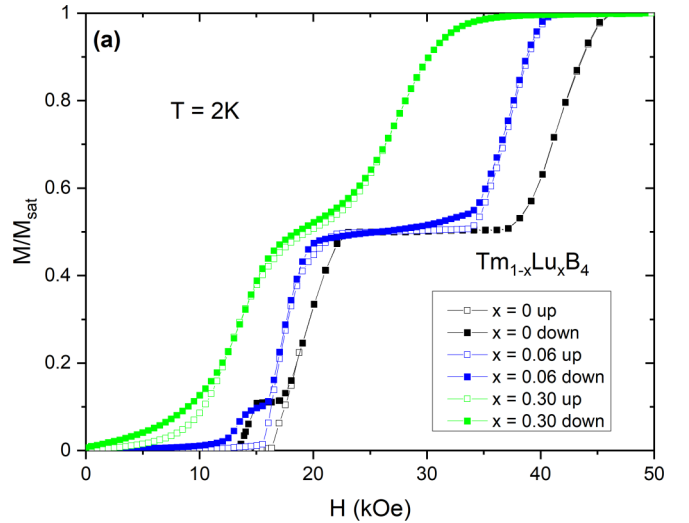


FIG. 2. (a) Magnetization curves measured at $T = 2 \text{ K}$. Empty points represent the field sweeps up, full points are the field sweeps down. (b) Temperature dependence of the heat capacity at zero magnetic field. The inset shows the dependence of Néel temperature $T_N(x)$ on the Lu concentration x .

measurements of magnetization and heat capacity. Magnetization curves of each sample were measured using the following protocol: the sample was first cooled in zero field to the base temperature of 2 K, then data points were collected while the field was ramped up to 50 kOe (with a stable field for each measured point); afterwards the field was ramped back to 0 kOe. Results are shown in Fig. 2(a).

In the case of pure TmB_4 ($x = 0$) in the virgin magnetization curve only the half plateau is observed, however, in the field sweep down also a fractional plateau emerges with magnetization value $1/9$ of saturated magnetization M_{sat} . In the literature also different fractions were reported ($1/7, 1/8, 1/9, 1/11$) depending on measurement conditions [12]. The solid solution $\text{Tm}_{0.94}\text{Lu}_{0.06}\text{B}_4$ exhibits a similar behavior, but in this case both plateaus are shifted to lower magnetic fields and become slightly “tilted.” For the heavily diluted system

with $x = 0.30$ both plateaus are smeared out and shifted to even lower magnetic fields.

The temperature dependence of the heat capacity at zero magnetic field is shown on Fig. 2(b). In the case of $x = 0.0$ and 0.06 two peaks corresponding to phase transitions are clearly visible, while for the concentration $x = 0.30$ only one distinct phase transition is observed. With increasing concentration of the Lu ions a decrease of the Néel temperature [inset of Fig. 2(b)] from $T_N = 11.7$ K for $x = 0.0$ to $T_N = 7.87$ K for $x = 0.30$ is observed.

B. Magnetocaloric effect of diluted TmB_4

The magnetocaloric effect in each sample was evaluated using the well-known procedure [31]. First, the entropy distribution was calculated from the temperature dependence of the heat capacity at constant magnetic field [31] using the relation

$$S(T)_H = \int_0^T \frac{C(T)_H}{T} dT + S_{0,H}, \quad (1)$$

where $S(T)_H$ is the temperature dependence of the entropy in a constant magnetic field H and $S_{0,H}$ is the entropy at zero temperature, which is set to zero [31]. For the missing experimental data in the temperature range between 0 and 2 K a linear extrapolation to zero temperature was used.

In the second step, from the obtained entropy distribution, the adiabatic temperature change ΔT was evaluated [31]:

$$\Delta T(T, H) = T(S)_{H=0} - T(S)_H, \quad (2)$$

where $T(S)_H$ is the temperature before demagnetization at an entropy S and $T(S)_{H=0}$ is the temperature after adiabatic demagnetization with the same entropy S . The resulting adiabatic temperature change for each sample is shown in Fig. 3.

In each case a large cooling region is observed, located in the paramagnetic state in a temperature range from 15 to 25 K and a field range from 30 to 46 kOe. Two heating regions are below the ordering temperature. With increasing concentration of Lu^{3+} ions a new heating region evolves in the paramagnetic phase. Interestingly, the largest adiabatic cooling temperature change $\Delta T = -12.75$ K is observed at the highest concentration of Lu^{3+} (i.e., the most diluted sample) whereas in the nondiluted case ($x = 0$) the maximum cooling effect is $\Delta T = -9.45$ K. For each case the refrigerant capacity was calculated using [31,32]

$$RC = \int_{T_1}^{T_2} |\Delta S| dT, \quad (3)$$

where T_1 and T_2 are the temperatures corresponding to both sides of the half-maximum value of the $-\Delta S$ peak, respectively. For cooling regions at 46 kOe, the RC values are $RC_{x=0} = 87.51$ J/kg, $RC_{x=0.06} = 88.78$ J/kg, $RC_{x=0.30} = 114.44$ J/kg. From these data it can be seen that the magnetocaloric properties of TmB_4 can be improved by dilution of the system.

C. Theoretical modeling of magnetocaloric effect

For the interpretation of the experimental data we have used the extended Ising model with additional interactions up to the fourth-nearest-neighbor spins on the SSL [30]. The

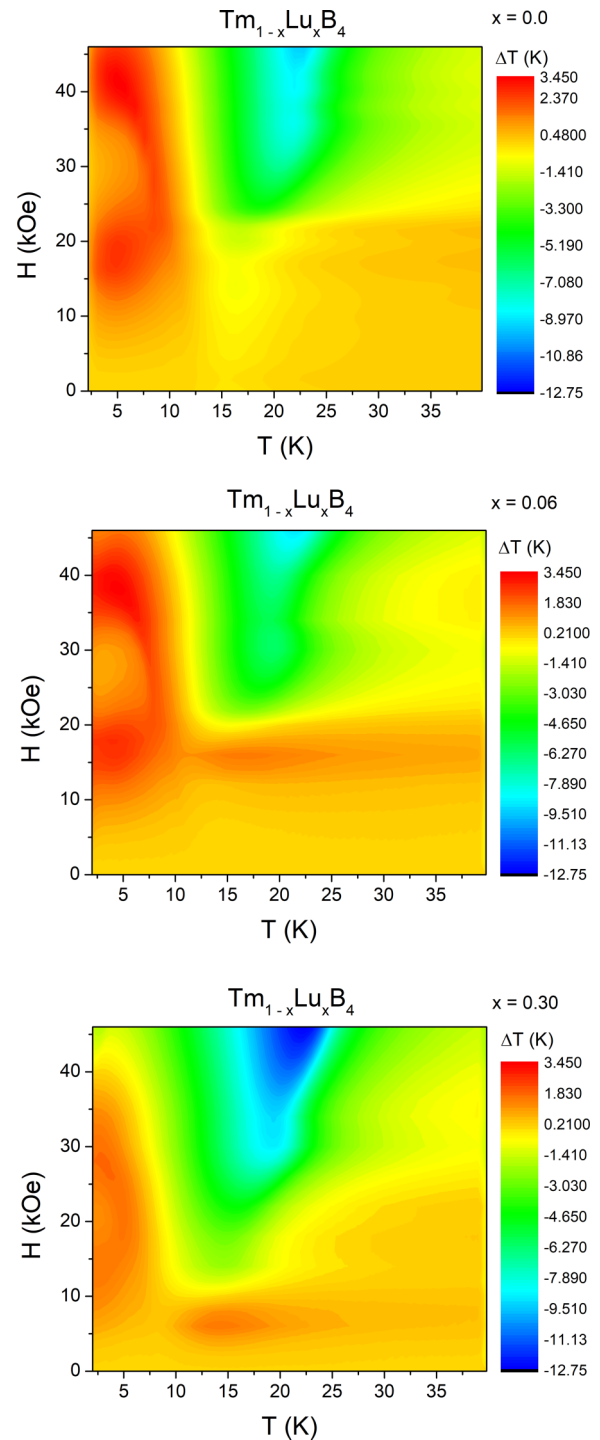


FIG. 3. The adiabatic temperature change ΔT , evaluated from heat-capacity measurements of $\text{Tm}_{1-x}\text{Lu}_x\text{B}_4$ ($x = 0.0, 0.06, 0.30$) single crystals. Data for the case $x = 0$ were taken from [26].

Hamiltonian of this system can be written as

$$\begin{aligned} \mathbf{H} = & J_1 \sum_{\langle i,j \rangle_1} S_i^z S_j^z + J_2 \sum_{\langle i,j \rangle_2} S_i^z S_j^z + J_3 \sum_{\langle i,j \rangle_3} S_i^z S_j^z \\ & + J_4 \sum_{\langle i,j \rangle_4} S_i^z S_j^z - h \sum_i S_i^z, \end{aligned} \quad (4)$$

where the J_1 , J_2 , J_3 , and J_4 are the exchange couplings between the first-, second-, third-, and fourth-nearest-neighbor spins on the SSL (in accordance with previous work [12,19,30], we set $J_1 = J_2 = 1$), S_i^z denotes the z component of a spin on site i of the real Archimedean lattice, and h is the magnetic field. In Ref. [30] the ground-state properties of this model have been studied by the classical Monte Carlo method using the standard Metropolis algorithm. Despite its simplicity this model was chosen because it provides a natural explanation for the stabilization of the single $1/2$ plateau

for a wide range of model parameters J_3 and J_4 . This half plateau was observed in experimental magnetization curves for various rare-earth tetraborides [10,15].

We have examined theoretically the measured magnetization and the MCE in undoped TmB_4 and in Lu-doped $\text{Tm}_{1-x}\text{Lu}_x\text{B}_4$ systems with $x = 0.06$ and $x = 0.30$. First, we calculate numerically the temperature dependence of the heat capacity $C = (\langle E^2 \rangle - \langle E \rangle^2)/(L/\tau)^2$ ($\tau = k_B T$) in various fields h , which were then used to evaluate the adiabatic temperature change. Using the same method as in [30] we

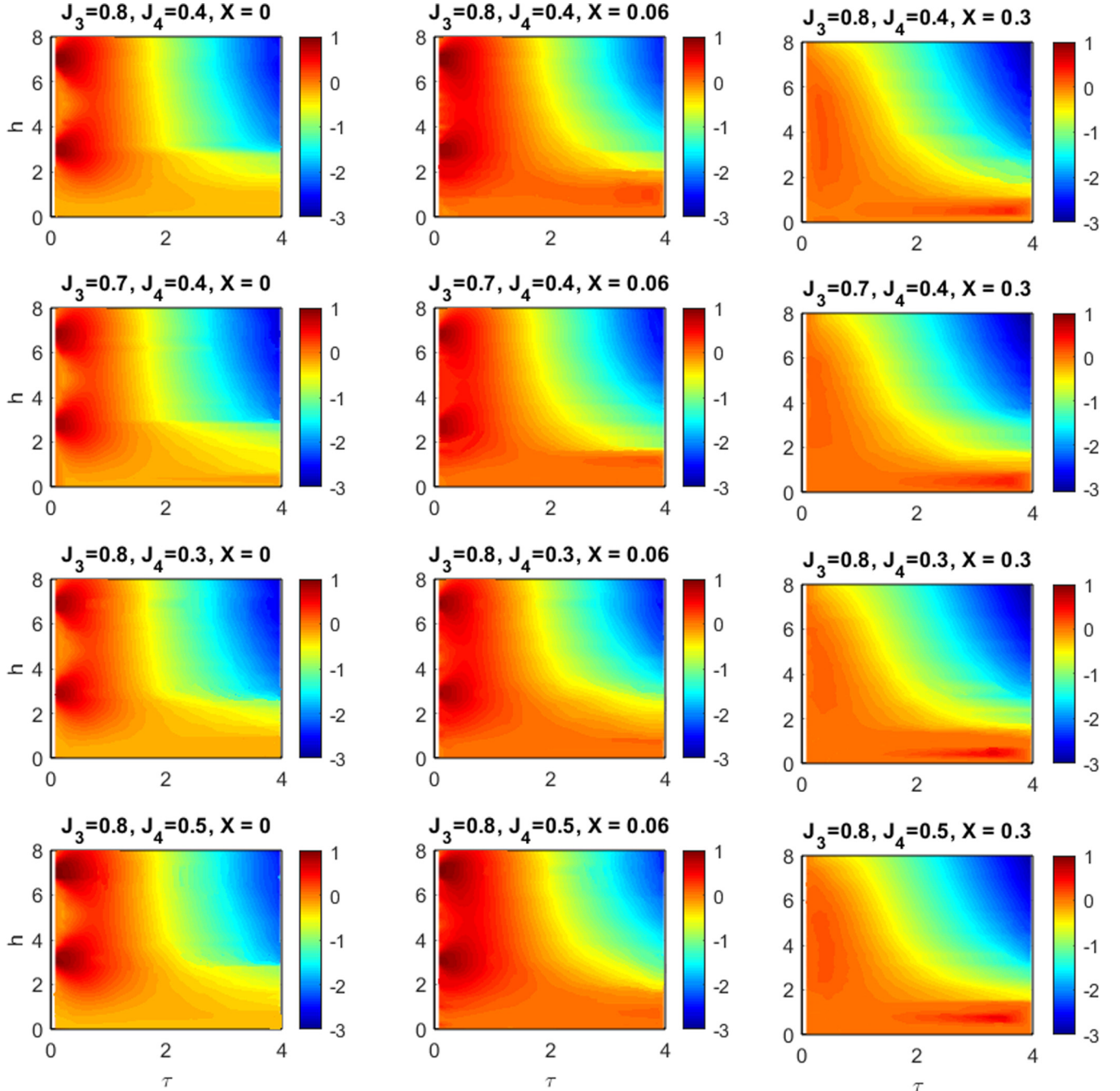


FIG. 4. Layout of the calculated adiabatic temperature change ΔT for a lattice of size $L = 10 \times 10$ for $x = 0, 0.06$, and 0.30 (columns from left to right) and different J_3 and J_4 parameters. The first row shows ΔT for optimum parameters (based on a comparison with Fig. 3). The other rows show the impact of deviations from optimum parameters.

have performed an extensive study of the model on clusters with $L = 10 \times 10$ and $L = 20 \times 20$ lattice points for a wide range of model parameters J_3 and J_4 , for which the model forms the main magnetization plateau $M/M_{\text{sat}} = 1/2$. To minimize the effects of Lu distribution, we have performed for each set of model parameters J_3 and J_4 n independent runs (typically $n = 100$) with random arrangements of the Lu atoms on the SSL.

A detailed analysis of our numerical results has shown that the layouts of adiabatic temperature change are very sensitive to the selection of model parameters. We have compared the numeric results with the experiment and find the best match for the parameters $J_3 = 0.8$ and $J_4 = 0.4$ for all three cases (the undoped system and systems with Lu concentration $x = 0.06$ and $x = 0.30$). The layouts of the adiabatic temperature change for $x = 0, 0.06$, and 0.30 and for low temperatures, where the magnetic contribution to entropy changes is dominant, are displayed in the first row of Fig. 4. For the undoped case ($x = 0$), we find two regions of heating at lowest temperature followed by the area of massive cooling at higher temperature. One can see that the area of cooling is almost the same for all cases. For the case of $x = 0.06$, both heating regions are slightly enlarged and another region of heating appears at higher temperatures ($\tau \sim 3$) and lower magnetic field ($h \sim 1$). In the case of $x = 0.3$, the two heating regions merge into one, but the temperature change in this region is significantly decreased. On the other hand, in the area of heating at $\tau \sim 3$ and $h \sim 1$, the temperature change is markedly increased.

In the next rows of Fig. 4, we show the layouts of the adiabatic temperature change for model parameters close to the best fit ($J_3 = 0.8$ and $J_4 = 0.4$). First, we show the effect of a small change of the model parameter J_3 ($J_3 = 0.7$ and $J_4 = 0.4$). Although the layouts for $x = 0$ and $x = 0.30$ have the same features as in the best-fit case, the region of heating at $\tau \sim 3$ is missing in the layout for $x = 0.06$. This region of heating for $x = 0.06$ does not appear either in the layouts for a small change of parameter J_4 ($J_3 = 0.8$, $J_4 = 0.3$ and $J_3 = 0.8$, $J_4 = 0.5$). Besides that, the large region of heating at the lowest temperatures is almost indistinguishable in the layouts of adiabatic temperature change for $x = 0.3$. These findings point to the fact that the $J_3 = 0.8$ and $J_4 = 0.4$ parameters can be considered to be the best model parameters for $\text{Tm}_{1-x}\text{Lu}_x\text{B}_4$ systems.

With known optimal interaction parameters, we have performed a study of the model for other concentrations x . From a practical point of view the cooling area at higher temperature is most interesting. For that reason, we have displayed in Fig. 5 the concentration dependence of the adiabatic temperature change for $\tau = 4$ and $h = 8$, where the cooling effect is the most significant. One can see that the adiabatic temperature change $\Delta\tau$ reaches a small maximum at the concentration $x = 0.02$, then the value of $\Delta\tau$ gradually decreases. This behavior is in agreement with the experiment shown in the inset of Fig. 5. Moreover, our theoretical results point to the fact that the maximum of the adiabatic cooling temperature change is achieved at concentration $x \sim 0.70$. Thus, the theoretical modelling identifies a concentration x at which the MCE is the most significant and shows that by dilution more effective magnetocaloric materials can be designed.

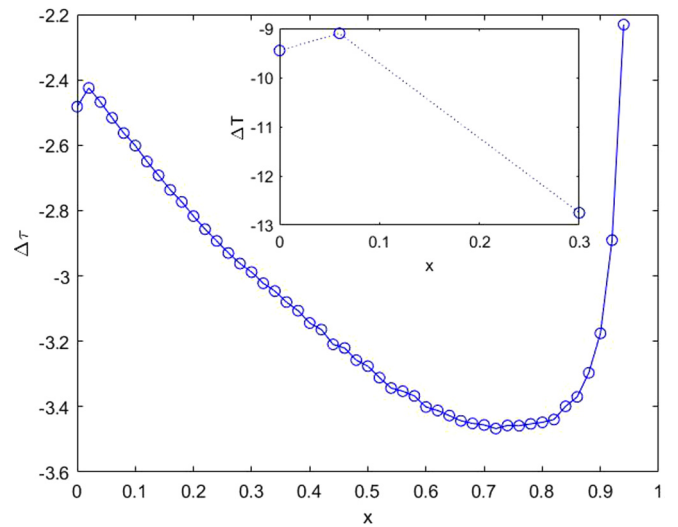


FIG. 5. The concentration dependence of the adiabatic temperature change $\Delta\tau$ for $\tau = 4$ and $h = 8$ numerically calculated from model Hamiltonian (4) and the largest experimentally measured adiabatic cooling temperature change ΔT (inset).

The behavior presented here seems to be a consequence of two opposite tendencies in the spin system. First, dilution by nonmagnetic ions generally relieves the massive degeneracy in frustrated systems (the ground-state entropy diminishes) and leads to a weakening of the magnetocaloric effect. On the other hand, sufficiently large (and not homogeneous) dilution causes the formation of small, independent (or nearly independent) magnetic clusters, which leads to a massive degeneracy of the ground state and thus to a significant entropy change. This change in entropy then causes an enhancement of the MCE. Similar results were also obtained in theoretical studies of Borovský *et al.* [33]. They were performed within the framework of an effective-field theory with correlations on a triangular Ising antiferromagnet, which was selectively diluted by nonmagnetic impurities. Their calculations led to an enhanced MCE at finite dilution and at sufficiently high temperatures.

Let us now discuss the effect of Lu concentration x on the magnetization curves for model parameters $J_3 = 0.8$, $J_4 = 0.4$ at low temperature ($\tau = 0.02$), which is presented in Fig. 6.

One can see that the calculated magnetization curves for x up to about 0.06 exhibit both features of the main $M/M_{\text{sat}} = 1/2$ plateau as well as features of the fractional $M/M_{\text{sat}} \sim 1/8$ plateau, which has also been observed in experiments. The magnetization curve for the higher concentration of Lu atoms (e.g., $x = 0.30$) is completely different—it exhibits only a continuous crossover from the low-field antiferromagnetic to the high-field ferromagnetic phase and all magnetization plateaus are absent. Although the magnetization curves behave different for the impurity concentrations in the simulation, they reach the saturation at the same value of magnetic field $h \approx 7$.

The results show that the theoretical model used here provides very good qualitative agreement with the experimental results. Within our study, it is quite straightforward to provide numerical calculations for arbitrary concentration x of Lu

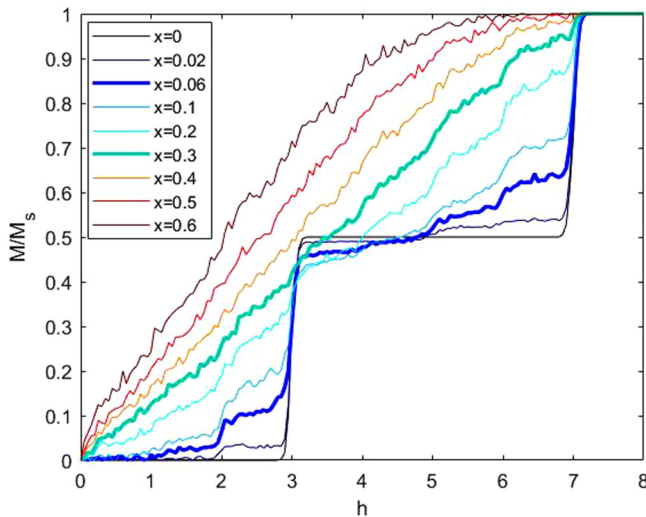


FIG. 6. Magnetization curves from Monte Carlo simulations of the Ising model on a SSL for $J_3 = 0.8$, $J_4 = 0.4$ for different values of x .

atoms in the $\text{Tm}_{1-x}\text{Lu}_x\text{B}_4$ systems. Such theoretical studies could help to optimize the parameter x where the magnetocaloric effect is most significant ($x \sim 0.70$) and thus it could contribute to the design of new magnetocaloric materials.

IV. CONCLUSION

We conclude that dilution of TmB_4 by nonmagnetic Lu^{3+} ions has a major impact on its magnetic and magnetocaloric properties. At low Lu concentration (up to $x \approx 0.06$) the magnetization plateaus shift to lower magnetic field; at higher concentration they gradually disappear. It also turns out that with the increase of x the adiabatic temperature change as well as refrigerant heat capacity can be increased. We used the extended Ising model with additional interactions up to the fourth-nearest-neighbor spins on the Shastry-Sutherland lattice to describe the observed experimental results. The model parameters were optimized to achieve the best match with obtained experimental results. The model with tuned parameters could be used to search for new, better magnetocaloric materials.

ACKNOWLEDGMENTS

This work was supported by the Slovak Research and Development Agency under Contract No. APVV-17-0020, by Project No. VEGA 2-0032-20, and by the DAAD-SAS Project No. 57452699. Liquid nitrogen for experiments was sponsored by U.S. Steel Kosice, s.r.o.

- [1] M. D. Kuzmin and A. M. Tishin, *J. Phys. D: Appl. Phys.* **24**, 2039 (1991).
- [2] O. Tegus, E. Brück, K. H. J. Buschow, and F. R. de Boer, *Nature (London)* **415**, 150 (2002).
- [3] Y. I. Spichkin and R. R. Gimaev, *Int. J. Refrig.* **37**, 230 (2014).
- [4] A. M. Tishin, Y. I. Spichkin, V. I. Zverev, and P. W. Egolf, *Int. J. Refrig.* **68**, 177 (2016).
- [5] V. Franco, J. S. Blázquez, J. J. Ipus, J. Y. Law, L. M. Moreno-Ramírez, and A. Conde, *Prog. Mater. Sci.* **93**, 112 (2018).
- [6] M. Zukovic and M. Semjan, *J. Magn. Magn. Mater.* **451**, 311 (2018).
- [7] W. N. Lipscomb and D. Britton, *J. Chem. Phys.* **33**, 275 (1960).
- [8] J. Etourneau and P. Hagenmuller, *Philos. Mag. B* **52**, 589 (1985).
- [9] S. Gabani, K. Flachbart, K. Siemensmeyer, and T. Mori, *J. Alloys Compd.* **821**, 153201 (2020).
- [10] F. Iga, A. Shigekawa, Y. Hasegawa, S. Michimura, T. Takabatake, S. Yoshii, T. Yamamoto, M. Hagiwara, and K. Kindo, *J. Magn. Magn. Mater.* **310**, e443 (2007).
- [11] S. Gabáni, S. Maťaš, P. Priputen, K. Flachbart, K. Siemensmeyer, E. Wulf, A. Efdokimova, and N. Shitsevalova, *Acta Phys. Pol. A* **113**, 227 (2008).
- [12] K. Siemensmeyer, E. Wulf, H.-J. Mikeska, K. Flachbart, S. Gabáni, S. Maťaš, P. Priputen, A. Efdokimova, and N. Shitsevalova, *Phys. Rev. Lett.* **101**, 177201 (2008).
- [13] S. Michimura, A. Shigekawa, F. Iga, T. Takabatake, and K. Ohoyama, *J. Phys. Soc. Jpn.* **78**, 024707 (2009).
- [14] S. Maťaš, K. Siemensmeyer, E. Wheeler, E. Wulf, R. Beyer, Th. Hermannsdörfer, O. Ignatchik, M. Uhlarz, K. Flachbart, S. Gabáni, P. Priputen, A. Efdokimova, and N. Shitsevalova, *J. Phys.: Conf. Ser.* **200**, 032041 (2010).
- [15] J. Trinh, S. Mitra, C. Panagopoulos, T. Kong, P. C. Canfield, and A. P. Ramirez, *Phys. Rev. Lett.* **121**, 167203 (2018).
- [16] D. Lançon, V. Scagnoli, U. Staub, O. A. Petrenko, M. Ciomaga Hatnean, E. Canevet, R. Sibille, S. Francoual, J. R. L. Mardegan, K. Beauvois, G. Balakrishnan, L. J. Heyderman, C. Rüegg, and T. Fennell, *Phys. Rev. B* **102**, 060407(R) (2020).
- [17] Z. Y. Meng and S. Wessel, *Phys. Rev. B* **78**, 224416 (2008).
- [18] M. C. Chang and M. F. Yang, *Phys. Rev. B* **79**, 104411 (2009).
- [19] Y. I. Dublennykh, *Phys. Rev. Lett.* **109**, 167202 (2012).
- [20] Y. I. Dublennykh, *Phys. Rev. E* **88**, 022111 (2013).
- [21] T. Suzuki, Y. Tomita, and N. Kawashima, *Phys. Rev. B* **80**, 180405(R) (2009).
- [22] T. Suzuki, Y. Tomita, N. Kawashima, and P. Sengupta, *Phys. Rev. B* **82**, 214404 (2010).
- [23] H. Čenčariková and P. Farkašovský, *Phys. Status Solidi B* **252**, 333 (2015).
- [24] Yu. I. Dublennykh, *Phys. Rev. E* **90**, 052123 (2014).
- [25] J. Shin, Z. Schlesinger, and B. S. Shastry, *Phys. Rev. B* **95**, 205140 (2017).
- [26] M. Orendáč, S. Gabáni, E. Gažo, G. Pristáš, N. Shitsevalova, K. Siemensmeyer, and K. Flachbart, *Sci. Rep.* **8**, 10933 (2018).
- [27] M. Orendáč, S. Gabáni, E. Gažo, G. Pristáš, N. Shitsevalova, K. Siemensmeyer, and K. Flachbart, *J. Magn. Magn. Mater.* **482**, 186 (2019).
- [28] M. Orendáč, P. Farkašovský, Ľ. Regeciová, K. Flachbart, S. Gabáni, E. Gažo, G. Pristáš, A. Dukhnenko, N. Shitsevalova,

- and K. Siemensmeyer, *Acta Phys. Pol. A* **137**, 764 (2020).
- [29] M. S. Song, K. K. Cho, B. Y. Kang, S. B. Lee, and B. K. Cho, *Sci. Rep.* **10**, 803 (2020).
- [30] P. Farkašovský and L. Regeciová, *Eur. Phys. J. B* **92**, 33 (2019).
- [31] V. K. Pecharsky and K. A. Gschneidner, *J. Appl. Phys.* **86**, 565 (1999).
- [32] H. Zhang, Y. W. Li, E. Liu, Y. J. Ke, J. L. Jin, Y. Long, and B. G. Shen, *Sci. Rep.* **5**, 11929 (2015).
- [33] M. Borovský and M. Žukovič, *Acta Phys. Pol. A* **131**, 645 (2017).